Evolution of Strain-Induced Microstructure and Texture in Commercial Aluminum Sheet under Balanced Biaxial Stretching

S.W. BANOVIC and T. FOECKE

The evolution of surface topography and crystallographic texture was investigated under balanced biaxial stretching in sheets of the aluminum alloy 5052-H32. Two different lots of material, with an initial nominal thickness of 1 mm, were tested in the as-received condition. Samples with increasing levels of balanced biaxial strain were deformed using a modified Marciniak in-plane stretching test. In general, the sheet materials were microstructurally and crystallographically anisotropic. Between the two lots, the initial microstructure and mechanical properties were found to be equivalent; however, the sheet texture was appreciably different. This latter variation was observed to have an effect on the additional roughening of the surface subsequent to deformation. For a given lot of material, the surface roughness was found to be proportional to the magnitude of the strain. However, while the roughening rates for the two lots were comparable, the lot having a stronger initial {220} texture component was found to roughen to a higher degree. Corresponding changes in the sheet texture were observed to have two regimes as a function of the strain level. In the first regime, typically, for strains (ε) up to 0.05, the orientations were found to rotate quickly away from the initial cube {001}⟨100⟩ orientation observed in the as-received sheet toward positions along the α fiber. Above a strain level of 0.05, the {220} texture component continued to increase with deformation, but at a decreasing rate up to failure of the sheet. The difference in the grain rotation rates observed did not appear to have an effect on the surface roughening, as the relative change of the crystallographic orientations with increasing plastic strain was similar for both heats of material. Instead, it is believed that localized grain or grain-grouping interactions may play a more important role in the surface roughening process.

I. INTRODUCTION

THE replacement of conventional steel sheet used for various automobile components with aluminum alloys would lead to reduced vehicle weight. This would provide one effective approach to reaching the gas-mileage goals set forth by the Partnership for a New Generation of Vehicles. However, widespread application of these lightweight materials by the automotive industry is presently limited, due to their poor formability in terms of limiting strains, wrinkling, and overall final surface appearance. These forming defects arise from both materials issues (*i.e.*, a limited number of slip systems for fcc aluminum compared to bcc ferritic steel; solution-strengthened aluminum alloys strain-rate soften, while steels strain-rate harden) and a lack of experience in forming aluminum. Automotive manufacturers are employing finite-element simulations to contend with these stamping problems by carrying out intensive die-design development prior to die fabrication. Unfortunately, this approach has been relatively unsuccessful at predicting the behavior of the material in terms of the complex stress states occurring within the sheet and the frictional forces occurring along the die-workpiece interfaces. This is believed to be a result of the *in-situ* development of surface roughness.

At room temperature, the surface roughness of aluminum alloys has generally been observed to increase in linear proportion to the magnitude of the plastic deformation[1–7] and to the average grain size,[4–9] but is independent of strain rate[4,5] and stress type (mode of deformation).[4–7,9] The predominant mechanism cited for the roughening process is associated with the different orientations of slip systems in adjacent grains.[2,4–7,10–13] This can lead to mismatch strains at the grain boundaries under multiaxial stretching. Upon deformation, neighboring grains, which typically have different crystallographic orientations, will deform by slip on particular crystallographic systems. The differences in the deformation of adjacent grains will lead to strain incompatibilities between them. As the effects of mutual constraint are partially relaxed at the free surfaces, the outermost grains are allowed to move normal to the surface to accommodate the strain at the grain boundaries, resulting in the formation of peaks and valleys. Thus, the higher the amount of deformation or the larger the initial grain size, the greater the surface roughness. The emergence of slip steps is thought to play a lesser role in roughening,[4,11] as their height magnitude is on a much smaller scale when compared to that of grain rotation.

Becker investigated the relationship between the initial crystallographic texture of an aluminum sheet and surface roughening as a result of deformation through detailed numerical simulations.[1] He observed that a sample with random grain orientations near the surface developed more roughening than sheets with higher-texture components, particularly those associated with the initially rolled texture. An important point found through the simulations was that

S.W. BANOVIC and T. FOECKE, Materials Research Engineers, are with the Metallurgy Division, National Institute of Standards and Technology, Gaithersburg, MD 20899-8553. Contact e-mail: swbanovic@nist.gov
Manuscript submitted November 29, 2001.

Table I. Alloy Compositions, as Mass Fractions Multiplied by 100, for the Two Lots of AA5052-H32 and the Acceptable Limits; Balance is Aluminum

Material	Mg	Fe	Cr	Si	Cu	Mn	Ni	Ti	Zn
Lot 1	2.50	0.40	0.22	0.23	0.10	0.09	0.01	0.05	0.06
Lot 2	2.30	0.28	0.21	0.13	0.06	0.02	0.01	0.01	0.01
Limits	2.2 to 2.8	0.40 max	0.15 to 0.35	0.25 max	0.10 max	0.10 max	—	—	0.10 max

a more uniform strain distribution occurred along the surface of the more highly textured materials as a result of strain variations between localized regions and the immediate surroundings being minimal. This resulted in less grain rotation, and, hence, the roughening of the surface decreased. This dependence of surface roughening on the neighboring grain misorientations suggests the possibility of reducing roughness by the development of certain textures within the sheet.[1,13,14] However, as Becker stated, the model used to obtain these results was not fully developed, as it is limited by its two-dimensional character. In addition, experiments indicating the effect of initial crystallographic texture on the surface roughness of an aluminum sheet, which could be used to assess the accuracy of the model, were not available in the literature. Thus, this article will focus on the experimental determination of the relationship between the initial, as-received microstructure and crystallographic texture of the sheet and the evolved surface roughness as a function of balanced biaxial strain.

II. EXPERIMENTAL PROCEDURE

The commercially available aluminum alloy 5052-H32 (in sheet form, of 1 mm nominal thickness) was received from two different suppliers. Table I gives the chemical composition for the two lots. Mechanical-property values were obtained through uniaxial tension testing for comparison of the as-received materials. These tests were conducted in accordance with ASTM E8-99, with the stress axis parallel to the rolling direction. Microstructures were revealed by mechanical polishing using 0.25 μm diamond paste, followed by a conventional anodizing technique using a solution of 2 mL of HBF and 98 mL of H_2O immersed in an ice bath. The samples were anodized for 45 to 60 seconds with a preset voltage of 30 V d.c. and were subsequently viewed using polarized light.

Equibiaxial deformation of the sheets was conducted using a modified Marciniak in-plane stretching test (Figure 1). This test was first proposed by Marciniak and Kuczynski,[15] and a detailed description of the experimental equipment used in this research can be found in Reference 16. This type of intrinsic testing was chosen over the more commonly used limiting-dome-height (LDH) test, so as to eliminate (1) the out-of-plane deflections associated with the bending/bulging of the sheet and (2) the unquantifiable frictional forces that exist between the sheet and punch.

Sample preparation of the as-received aluminum sheets consisted of cutting to a 30 × 30 cm sample size. In order to remove both the native oxide layer and remnants of the deformation marks that developed during the rolling procedure, a central portion of one face was polished to a 6 μm diamond finish. Cleaning was subsequently done using acetone and cotton. After preparing the surface to
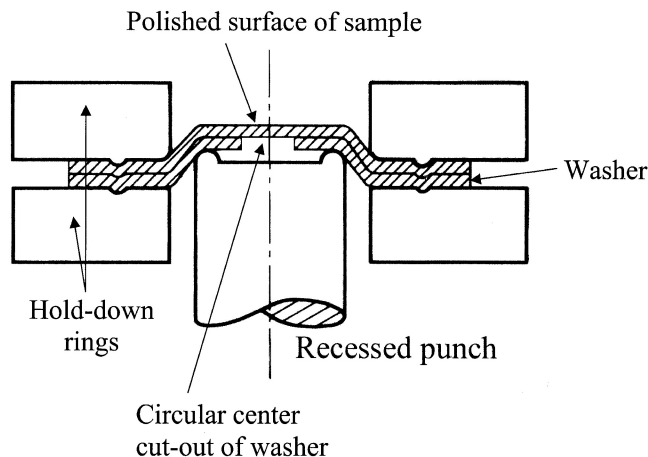

Fig. 1—Schematic of the modified Marciniak in-plane stretching test.

the 6 μm diamond finish, the sheet thickness averaged 0.98 mm. A circle with a 28 mm diameter was stenciled in the exact center of the sheet for strain determination.

Drawing quality–special killed steel, with dimensions of 30 × 30 × 0.1 cm, was used as a washer (driver blank) to prevent failure in the sidewall of the aluminum test sheet. A 10-cm-diameter center cut out of the blank was used to maximize the area of uniformly, biaxially strained test material. The washer was placed between the Marciniak tooling and the aluminum sheet, with the unpolished side of the sample in contact with the washer (Figure 1). Lubricant was placed on the sides in contact with the tooling. This configuration for testing resulted in a 15-cm-diameter area (the central portion of the specimen, which remained flat and free from any frictional forces) that was uniformly deformed in an equibiaxial mode with an unmarred sheet face for surface characterization. The load of the hold-down ring was maintained at approximately 340 kN for the duration of testing, so that movement of material inward over the draw bead was restricted. A constant central ram speed of 0.5 mm/s was used for testing, and the ram load was observed to remain below 320 kN. Varying amounts of stretching were obtained by setting the limit control of the central ram (Marciniak tooling) to predetermined deflections. The true in-plane strain was determined by measuring the change in diameter of the stenciled circle along three directions: parallel, perpendicular, and 45 deg to the rolling direction of the sheet. The true through-thickness strain was calculated after measuring the final sheet thickness, using calipers with a resolution of ± 20 μm.

Pre- and postcharacterization of the aluminum sheet consisted of measuring both external and internal characteristics of the material. Changes in the surface topography of the polished face were observed through roughness measurements *via* a mechanical stylus profilometer fitted with

a 5-μm-diameter probe tip. A minimum of 15 traces per sample was conducted, with a trace length of 5.6 mm and a 0.8 mm cutoff length. Measurements were made along three directions of the sheet: parallel, perpendicular and 45 deg to the rolling direction. The parameters of the arithmetical mean of the areas of all profile values of the roughness profile (R_a) and the vertical distance between the highest peak and the deepest valley of a single roughness profile (R_y) were chosen to characterize the surface; however, it is recognized that these parameters do not give a complete description of the roughness of a surface. Scanning electron microscopy of the surface was also conducted to determine the change in surface topography.

The texture of the sheets was evaluated using neutron diffraction, X-ray diffraction, and electron-backscattered diffraction (EBSD) techniques. The neutron-diffraction studies were conducted at the NIST Center for Neutron Research. For these experiments, sample sizes were 5 mm on a side, stacked five high, which resulted in the beam irradiating approximately 125 mm^3 of deformed material. The samples were mounted in the center of a four-circle diffractometer with the rolling direction parallel to the beam (wavelength of 1.884 Å). The pole-figure data of the three reflections ({111}, {200}, and {220}) were measured over an entire orientation hemisphere ranging from 0 deg to 360 deg in ϕ angle and 0 deg to 90 deg in χ angle, each in 5 deg steps using standard procedures.[17]

The X-ray diffraction technique used to obtain the texture along the rolling direction of the sheet is described in detail in References 18 and 19. A conventional powder X-ray diffractometer was used for both scan collections (θ-2θ scans and θ scans) with incident and receiving slits of 0.68 and 0.53 deg, respectively. The tube electric current was 40 mA at a voltage of 45 kV. These conditions resulted in a sampled area of 225 mm^2 across the surface at a maximum depth of approximately 50 μm, thus allowing for a large area of the surface to be analyzed. Rocking curves, or ω scans, for the {111}, {200}, and {220} reflections were obtained by correcting the θ scans for defocusing and absorption using the WINDOWS*-based software package

*WINDOWS is a trademark of the Microsoft Corporation, Redmond, WA.

called TexturePlus, which is available on the World Wide Web.[20]

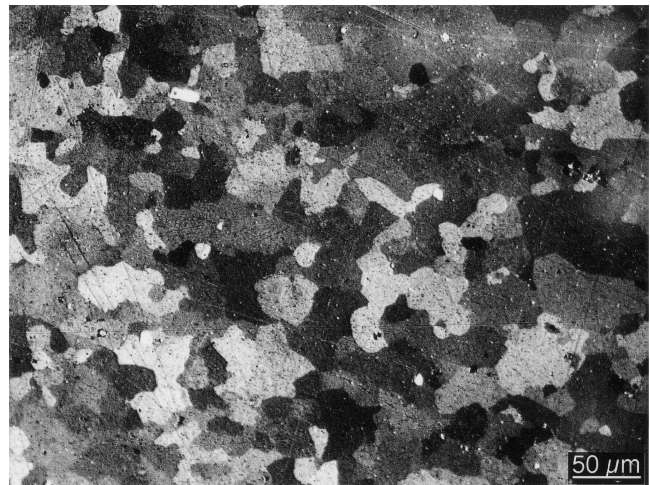For the EBSD technique, a JEOL* 6400 scanning electron

*JEOL is a trademark of Japan Electron Optics Ltd., Tokyo.

microscope with a tungsten filament was used, with settings of 20 kV, a magnification of 750 times, and a working distance of 28 mm. The samples were tilted 68 deg with respect to the beam. Scans were collected using the Channel 5 software from HKL Technologies, with subsequent generation of pole figures and orientation distribution functions from the data.
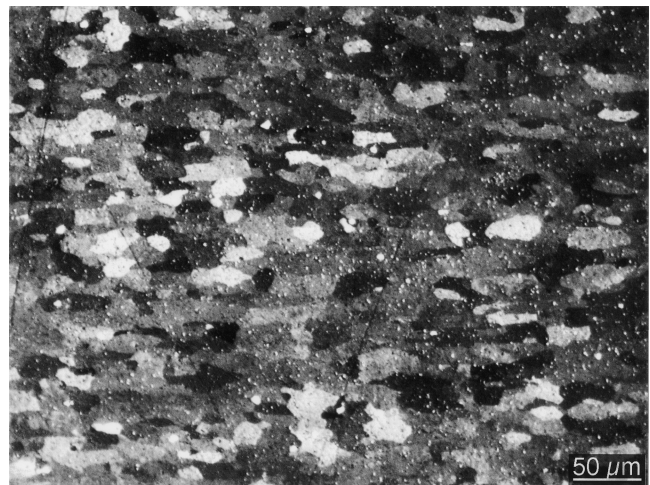
III. RESULTS

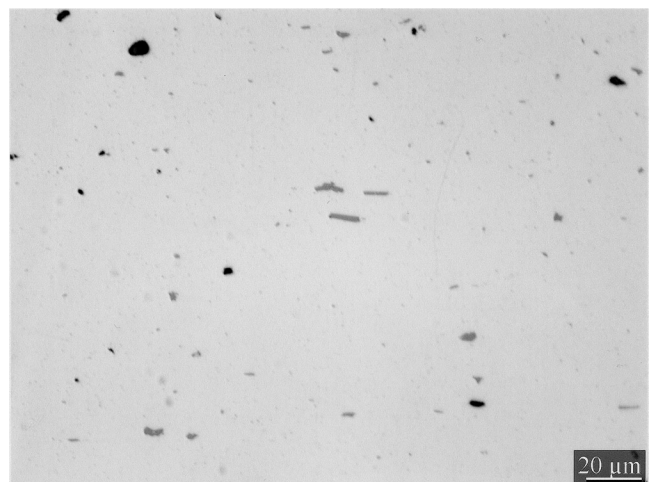### A. *Microstructural Characteristics*

As-received materials from the two different lots of AA5052-H32 were found to have similar microstructures

(*a*)

(*b*)

(*c*)

Fig. 2—Microstructures of material from lot 1: (*a*) short transverse direction, (*b*) long transverse direction, and (*c*) second-phase constituents in the short transverse direction.

(Figure 2) and mechanical properties (Table II). Figure 2(a) shows the relatively equiaxed grains in the short-transverse direction (plane of the sheet) that were elongated when

Table II. Comparison of Mechanical Properties for the Two Lots of AA5052-H32

	0.2 Pct YS (MPa)	UTS (MPa)	Total Uniform Elongation (Pct)	Total Elongation (Pct)
Lot 1	182 ± 8	239 ± 5	8.1 ± 0.6	9.5 ± 0.5
Lot 2	185 ± 7	242 ± 4	8.0 ± 0.6	10.0 ± 1.0
Typical	195	230	—	12

Table III. Average Planar Grain Size (in the Short Transverse Direction) and Transverse Aspect Ratio for Samples of Various Strain Levels

	Average Planar Grain Size (μm)	Transverse Aspect Ratio
0.0 (as-received)	31 ± 9	1.9 ± 0.5
0.104	35 ± 13	4.0 ± 0.5
0.198	41 ± 14	7.2 ± 1.7

Fig. 3—Plot of through-thickness strain *vs* in-plane strain for AA5052-H32.

examined in the long-transverse direction (Figure 2(b)). Table III gives the average planar grain size, as determined by the linear-intercept method, and the aspect ratio for the long-transverse direction. There was no statistical difference in grain size between the two lots of material. However, based upon Figures 2(a) and (b), the anisotropy of the sheet on a microstructural basis was evident.

Second-phase constituents were found to be dispersed throughout the matrix as well as in the grain boundaries (Figure 2(c)). There was no significant difference noted between the two lots. As both lots of material fell within the acceptable composition range for the commercially available sheet, further analysis of the particles was not conducted. However, the size, shape, and coloring suggested that they were most likely $(FeCr)_3SiAl_{12}$, Mg_2Si, and other intermetallic phases typically found in the 5*xxx*-series alloys.[31]

Postdeformation analysis revealed that the grain shape was found to have further elongated, when the microstructure was examined in the long-transverse direction. Table III shows that while the average planar grain size did not dramatically change, the transverse aspect ratio was found to increase significantly.

B. Marciniak Testing

Figure 3 shows the through-thickness strain of the samples, calculated from the thickness measurements, as a function of the in-plane strain. A linear relationship was observed between the two measurements, consistent with the constraints of volume conservation. The individual in-plane strain level for each sample was found to be extremely uniform across the area of interest. Also, the initial anisotropy of the sheet was not observed to affect the formability of the sheet, below the limiting strain, as there was no statistically significant difference in the in-plane strain measured along the three directions. The variability between the two lots of material was also negligible.

A limiting strain of 0.21 ± 0.01 was found for this material, while published values obtained using the LDH test report a strain of approximately 0.30.[32] This difference
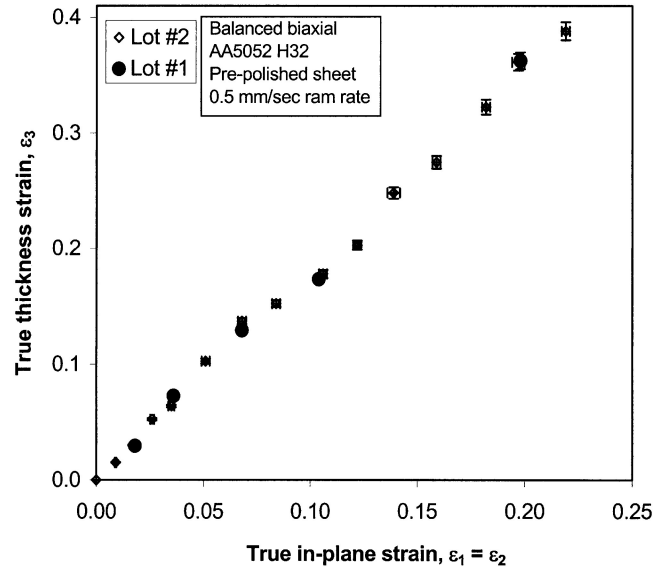
can be attributed to the relatively large amount of material (approximately 180 cm^2) which was sampled *via* the current method. This allows more defects in the material to be sampled, leading to a higher probability of failure at lower strains. Also, it has been shown that out-of-plane straining, which occurs during the LDH test, is different from the in-plane straining due to the effects of curvature, normal pressure, and friction from the tooling.[33] These factors may retard the *in-situ* formation of defects in the sheet and can lead to higher limiting strains during out-of-plane deformation when compared to values obtained *via* in-plane techniques.[34] When failure of the sheet did occur, the fracture was primarily oriented parallel to the rolling direction and initiated within the center of the sample (away from the area where the ram was in contact with the specimen). Failure of the sheet along this path was anticipated, as more defects (thickness variations) and microstructural variations (elongated grains and second-phase constituents) are expected to be aligned parallel to the rolling direction. Also, since failure occurred away from the edges of the sample, the intrinsic strength of the material was tested, and extraneous variables from the testing procedure were not found to influence it. For some samples, the test was halted prior to the fracture reaching the edge of the sample. In these circumstances, wide and deep grooves (on the order of 1 and 0.3 mm, respectively) were observed in the areas directly ahead of the fractured regions.

C. Surface Roughness

During the stretching process, the sample went from having a mirror-like finish to having a hazy appearance as the amount of deformation increased. Qualitatively, there was a transition around a strain level of 0.05, in which one could no longer make out clear features in the reflection off the sheet. As mentioned previously, failure of the sheet was preceded by the formation of small undulating grooves across the surface that were consistently oriented parallel to the rolling direction. These features did not occur until the final stages of straining (levels above 0.20), after which they
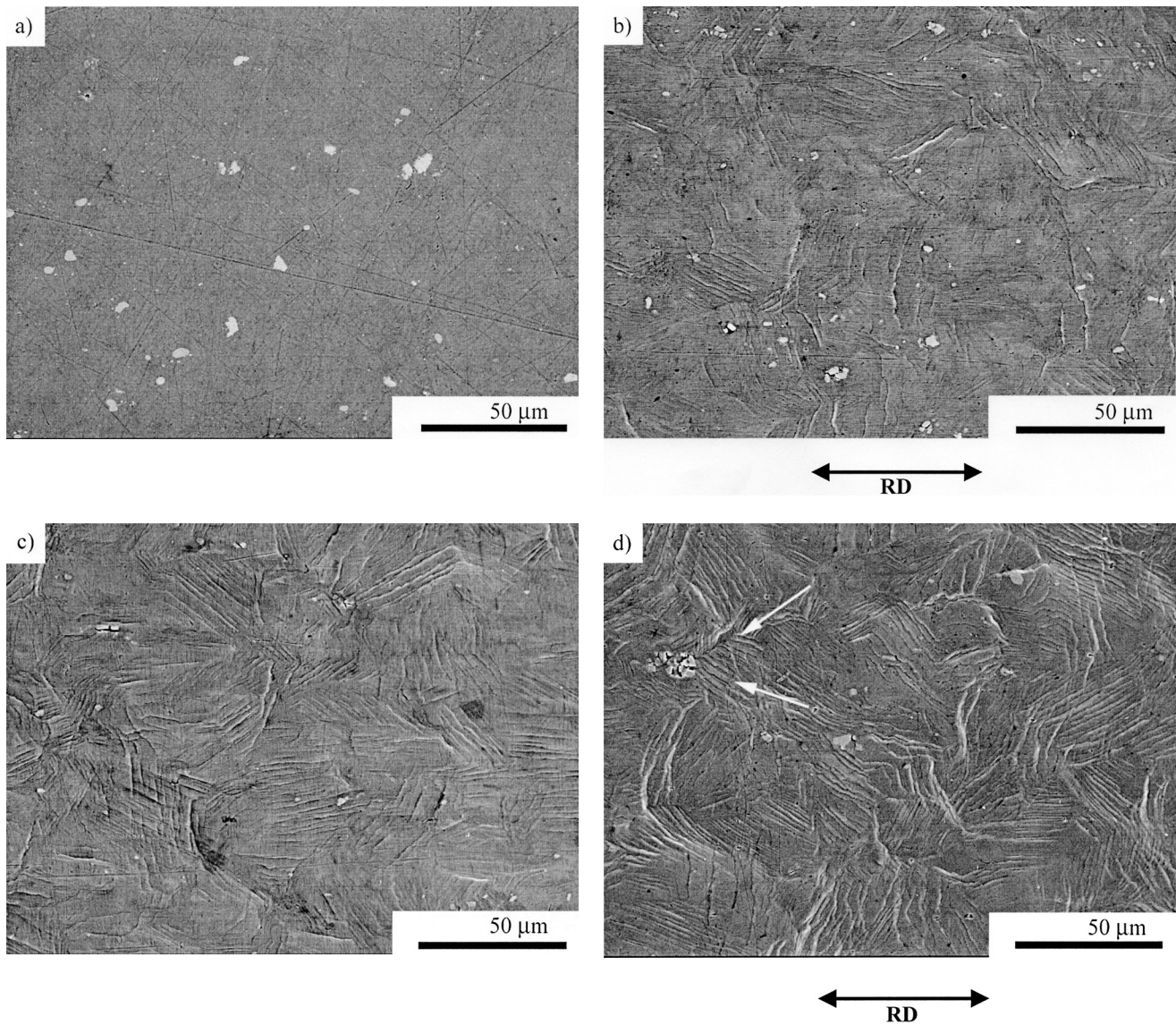
Fig. 4.—Secondary electron micrographs revealing the evolution of surface topography on the free surface as a function of the in-plane strain for material from lot 1. The strain levels shown are (*a*) 0.0 (polished sheet), (*b*) 0.051, (*c*) 0.104, and (*d*) 0.198. Arrows in (*d*) point out the near vertical lines discussed in the text.

developed into diffuse grooves across the surface. Failure of the sheet typically resided within one of these grooves.

Microscopically, the evolution of surface topography on the free, polished surface was tracked as a function of the strain level using scanning electron microscopy. Figure 4 shows this evolution for samples from lot 1. The polished sheet (Figure 4(a)) shows the second-phase constituents as well as some light, straight scratches on the surface from the polishing procedure. As the material was progressively deformed in a balanced biaxial mode, slip bands began to emerge out of the surface and were readily apparent, at this resolution, after a strain level of 0.026. Initially, the slip bands were not homogeneously distributed across the structure, in terms of their number, dispersion, or severity (height), as localized regions appeared devoid of the deformation marks (Figure 4(b)). With larger strains, the slips steps were found to be more uniform across the surface and their number and height increased (Figures 4(c) and (d)). There was no apparent orientation relationship between the

slip lines and the rolling direction, as their orientation was randomly distributed on the surface, similar to the results of Guangnan *et al.*[2] In terms of their appearance, the slip bands had a "wavy" characteristic (according to the definition of Williams *et al.*,[35] *i.e.*, bands which are broad, diffuse, branched, or curved), which would be indicative of a cross-slip mode of deformation. While transmission electron microscopy observations were conducted to confirm or refute the occurrence of cross slip, the results were inconclusive.

Images with increased magnifications of samples with higher strain levels showed further evidence of the change in the surface. Figure 5(a) shows either a grain or group of grains that have moved normal to the surface, producing peaks and valleys. With continued deformation, the differences between the peaks and valleys intensified as the latter became deeper and wider. Both decohesion and cracking of the second-phase constituents was noted (Figure 5(b)) for strains as low as 0.018. Also of particular interest was the
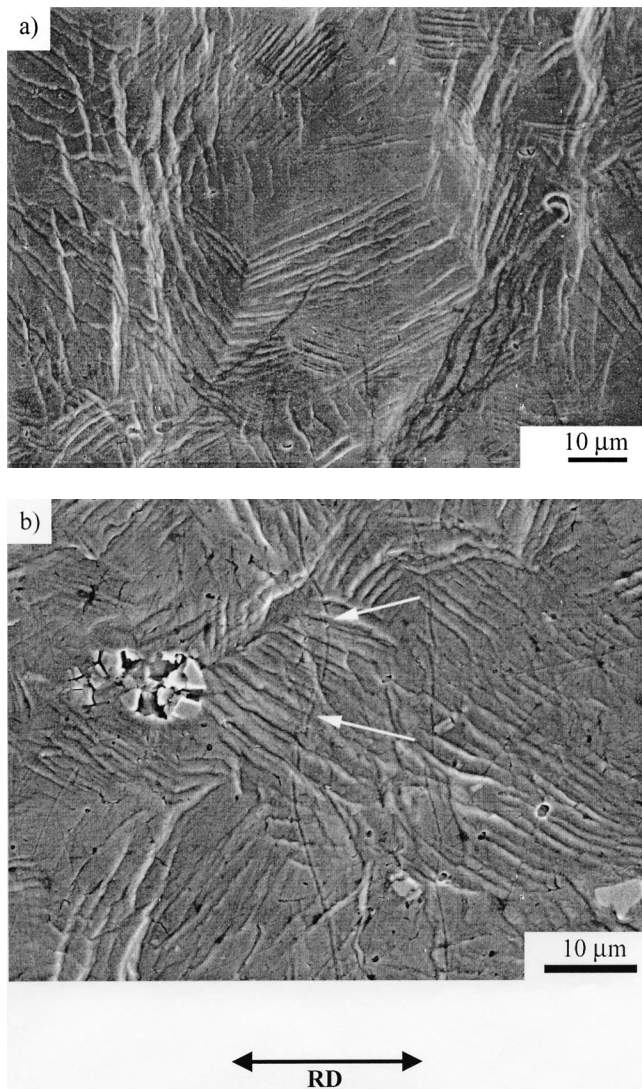
Fig. 5—Secondary electron micrographs of (*a*) a grain or a group of grains that have shifted normal to the surface producing peaks and valleys and (*b*) decohesion and cracking of the second-phase constituents next to the initially straight polishing scratch (lot 1 material with a strain level of 0.198).

appearance of the initial scratch lines produced from the 6 μm diamond polish. In all cases observed, these scratches were fairly straight prior to deformation (Figure 4(a)). After deformation of the sample, these lines also took on a wavy appearance. Note the scratch running near vertical in Figure 4(c) and in the higher-magnification image in Figure 5(b). This change in appearance would be indicative of a change in the surface topography.

To corroborate the change in surface characteristics, roughness parameters were quantified as a function of the in-plane strain level. Figures 6(a) and (b) display the R_a and R_y values for the deformed material from lot 2. With the exception of the lowest strain levels, there was no significant difference between the measurements along the three directions. The lower strain levels were found to have variations, as the remnants from the initial rolling marks were not completely removed during the polishing procedure. This resulted in higher values for the probe traces perpendicular to the rolling direction. However, this deviation was not seen to affect the data after a strain of 0.018. From the data

obtained along the three directions, averages were calculated and comparisons made between the two lots of material (Figures 6(c) and (d)). The plots showed that for equivalent strains, the roughness measurements of material from lot 1 were consistently lower than those obtained from lot 2. The individual roughening rates calculated for the materials are located in Table IV and do not show a significant difference. In addition, it appears that the roughness values may be saturating near the limiting strain, above strain levels of 0.20.

For samples that failed and had diffuse grooves ahead of the crack tip, roughness measurements were made in the valleys, parallel to its length. These values were found to be higher than those obtained for material outside of the groove (diamond symbols in Figures 6(c) and (d)).

D. *Crystallographic Texture*

The pole figures obtained from neutron-diffraction techniques are shown in Figure 7 for strain levels of 0, 0.104, and 0.198 from material of lot 1. Similar intensities were observed for lot 2. The as-received material (Figure 7(a)) displayed a strong {200} component. With increasing strain in the material, the development of a prominent {220} component and the decrease of the {111} and {200} components were observed. In addition, planes of the form {200} were found to be more uniformly dispersed along the rim of the projections after deformation (Figure 7(c)), indicating a more homogeneous distribution of ⟨200⟩ components that were parallel to the plane of the sheet than in that seen in the as-received condition (Figure 7(a)). The asymmetry of the plots indicates the anisotropy of the sheet on a crystallographic basis.

X-ray Θ-2Θ scans of the as-received material showed a variation in the initial texture of the two lots (Figure 8). An average difference of approximately 30 pct in the maximum intensity of the individual peaks was found, with material from lot 2 initially having a stronger {220} component.

The subsequent rocking curves obtained for both lots were found to replicate the trends of the neutron-diffraction data (Figure 9). These ω scans were taken from lot 1 material and are aligned parallel to the rolling direction. Therefore, the line A-B in Figure 9(b) corresponds directly to the line A-B on the {200} pole figure, shown as an example in Figure 7(c). Due to the configuration of the X-ray equipment, only partial scans (*e.g.*, from 0 deg to $\pm$31 deg for the 220 peak) could be obtained and not the full scans along the line A-B (0 deg to 90 deg), as acquired for the neutron results. However, values taken from the symmetric position ($\omega = 0$ deg) again showed that an increase in strain led to a decrease in grains oriented with their ⟨111⟩ and ⟨200⟩ components normal to the sheet plane, while the overall number of grains with their {220} components parallel to the plane of the sheet increased.

When comparing the rocking curves between the two lots of material, it was observed that equivalent amounts of strain did result in similar texture profiles, but the intensities of the scans were different. Figure 10 shows the average intensity values for the symmetric position ($\omega = 0$ deg) for both sets of materials as a function of the strain level. The offset in intensities was associated with the difference in initial texturing of the materials, as seen in Figure 8. While direct comparison of these average intensities at $\omega = 0$ deg could not be made, quantitative changes in the orientation of the
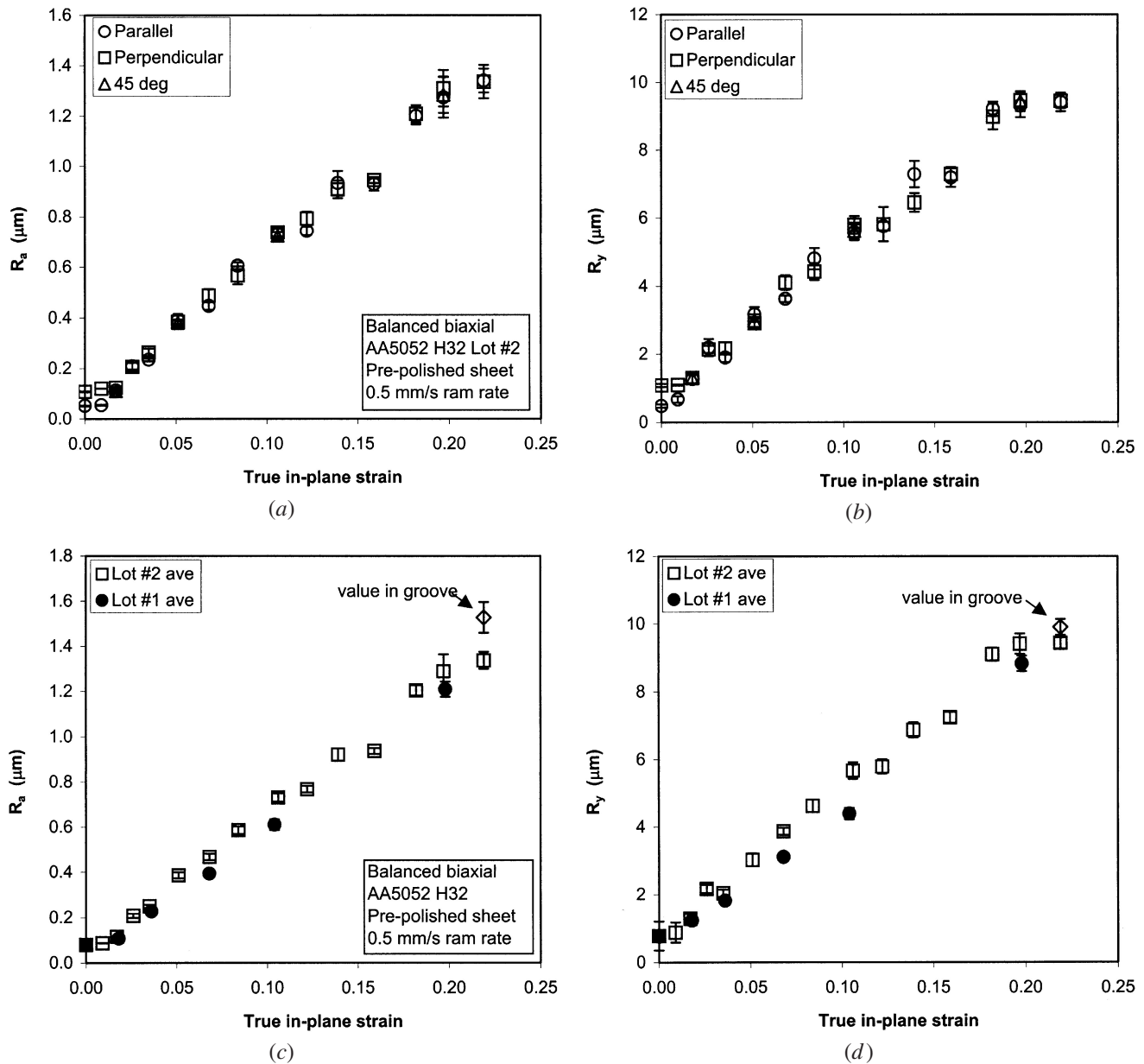
Fig. 6—Roughness parameters as a function of the in-plane strain level. (*a*) and (*b*) Results obtained for lot 2 along three directions. (*c*) and (*d*) Averaged values for the three directions plotted and compared between the two lots of material. The values obtained in the diffuse grooves ahead of the crack tip are also shown as diamonds.

Table IV. Roughening Rates, in $\mu m/\varepsilon_p$, for the Two Lots of AA5052-H32 as Calculated from Figure 5; Correlation Coefficients for the Fit of the Data Are Also Indicated

	R_a		R_y	
	Roughening Rate	Correlation Coefficient	Roughening Rate	Correlation Coefficient
Lot 1	5.9	0.99	41.0	0.99
Lot 2	6.1	0.99	42.6	0.98

sheets, when compared to their initial intensities, could be evaluated. The absolute values of the changes in the maximum intensities at $\omega = 0$ deg are shown as a function of the strain level in Figure 11 for the three reflections. In general, the data for both lots appear to lie along the same

curve, with a break in the slope between strain levels of 0.04 to 0.05. The rate of texture development (**R**) for these two regimes can be found by determining the slopes of the two portions of the curve (Table V), with the initial slope about 5.5 times larger than the latter.

Orientation distribution functions were generated from the EBSD data collected. Examples from lot 2 material are found in Figure 12 for strain levels of 0.0 and 0.219. The as-received material shows the cube $\{100\}\langle001\rangle$ rolling-texture component typically developed during processing of fcc materials.[28] As the material is deformed, the grains are observed to rotate toward positions along the alpha fiber, defined as common orientations with the $\langle110\rangle$ component normal to the plane of the sheet. There appears to be a strong concentration near the brass $\{110\}\langle112\rangle$ component. Similar results were obtained for lot 1 material.
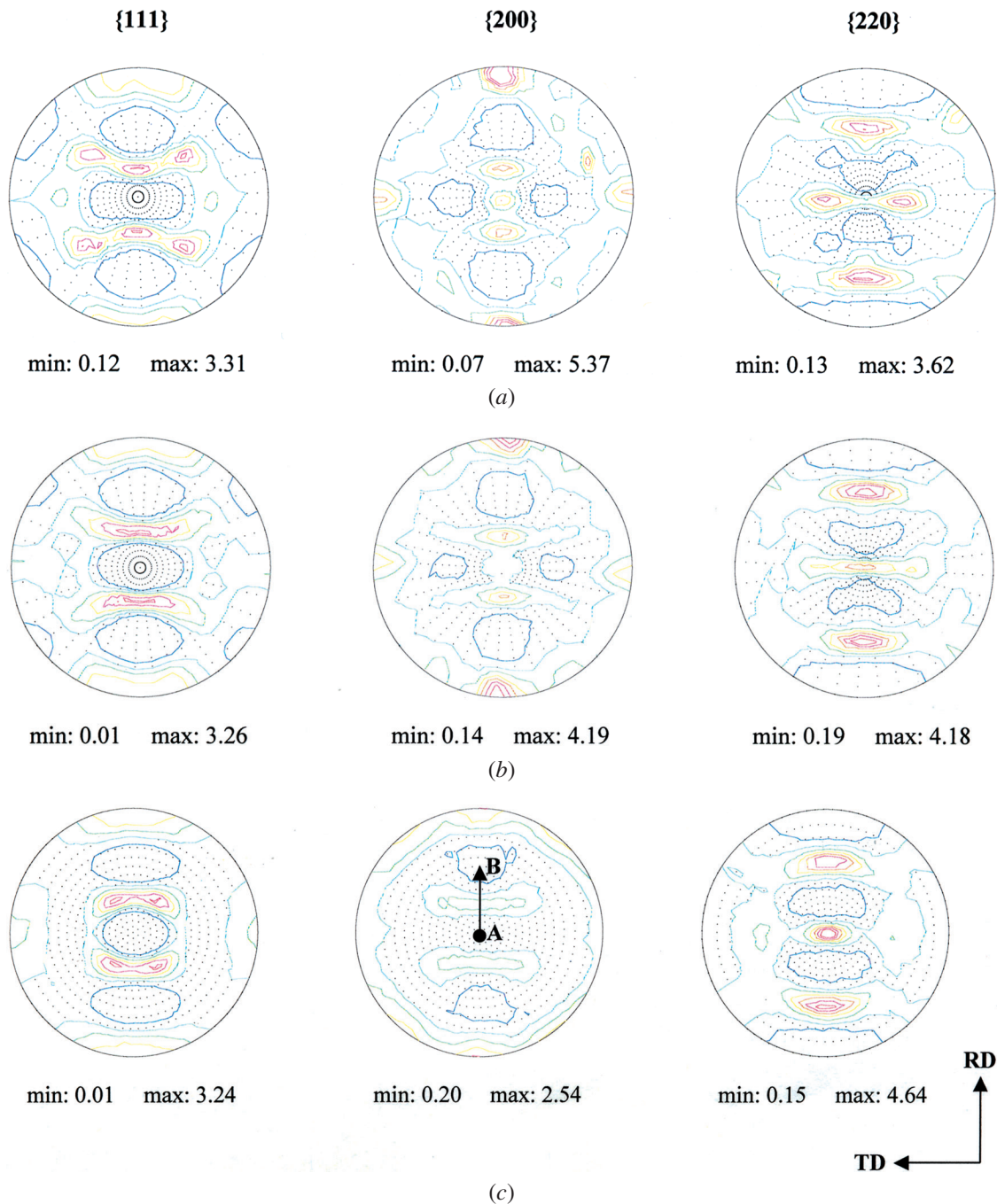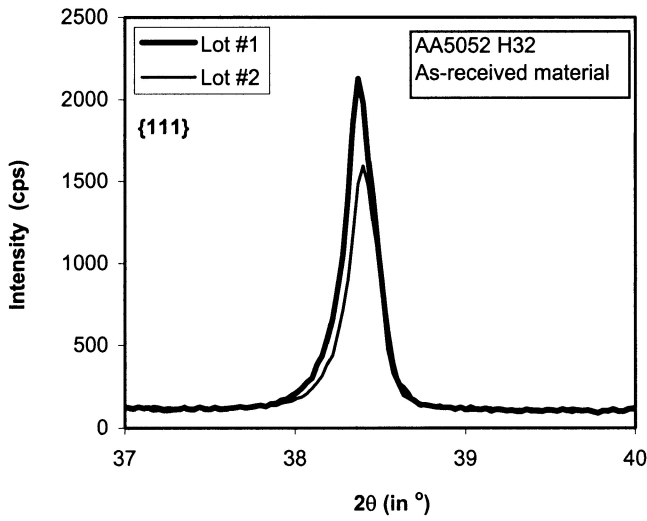
Fig. 7—Pole figures obtained *via* neutron diffraction for strain levels of (*a*) 0.0, (*b*) 0.104, and (*c*) 0.198 from material of lot 1. Isolines are 0.5 to 6.0 in steps of 0.5 with their minimum and maximum values indicated. The rolling and transverse directions are shown. The line A-B in the {200} reflection for the sample with 0.198 indicates the slice of data acquired by the X-ray diffraction technique.
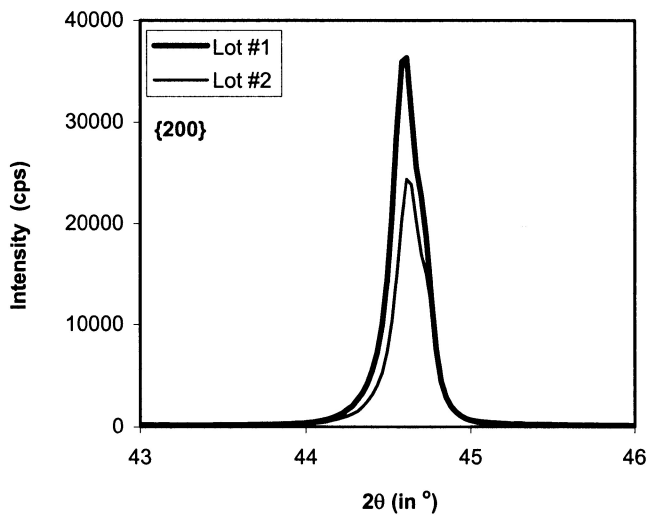
IV. DISCUSSION

In this research, commercially available aluminum sheet was tested in the as-received condition to determine the relationship between strain levels and evolving surface roughness and sheet texture. The sheets were manufactured by a combination of mechanical working and thermal treatments and, thus, are anisotropic in both the microstructural and crystallographic sense. Microstructural anisotropy is typically caused by variations in the grain size or shape, while crystallographic anisotropy arises from some preferred orientation or texturing of the grains in the material. Both
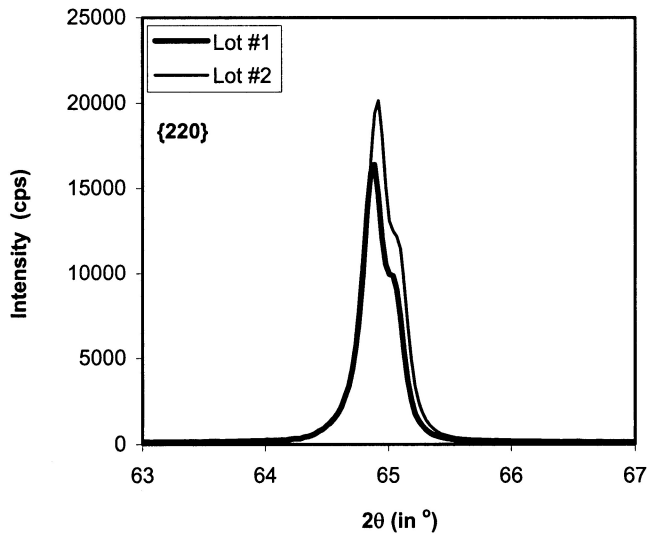
of these factors rely heavily upon the composition of the alloy and the processing parameters (*e.g.*, rolling temperatures, amount of deformation, and postheat treatment) of the sheet. However, it has been suggested that the deformation texture may change only slightly from the as-received texture during the stretching process, as the amount of deformation is limited.[21] If this is the case, then it is important to study the impact of the anisotropy from the initial texture, inherited from the rolling process, on the evolved surface roughness and developed strain texture of the sheet subsequent to deformation. The activation of slip systems and the rotation of
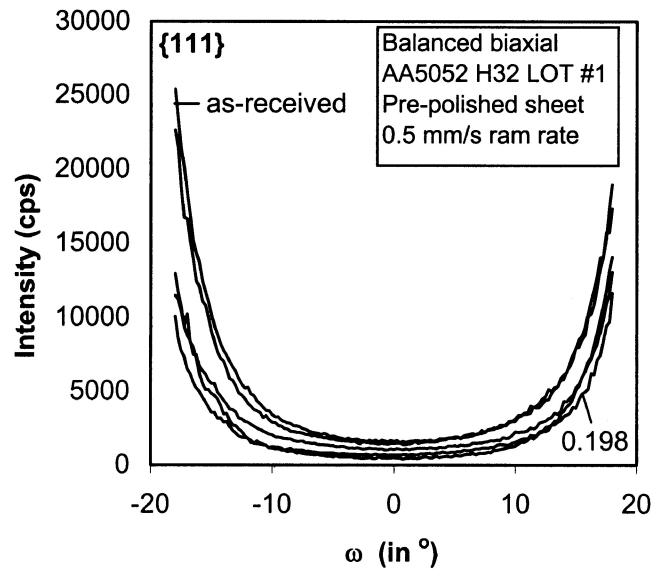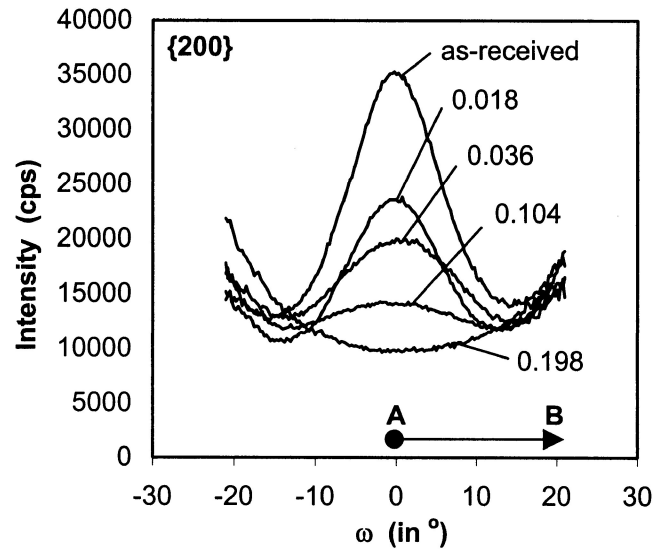
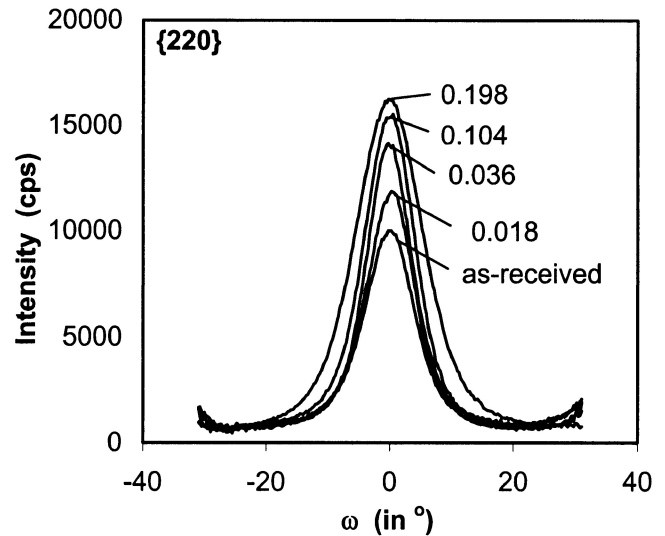Fig. 8—(a) through (c) Portions of θ-2θ scans, acquired with X-ray diffraction techniques, of the as-received material showing a variation in the initial texture of the two lots.
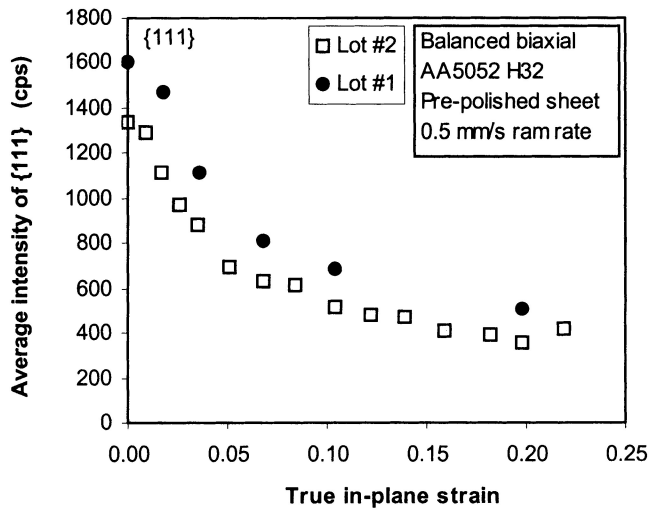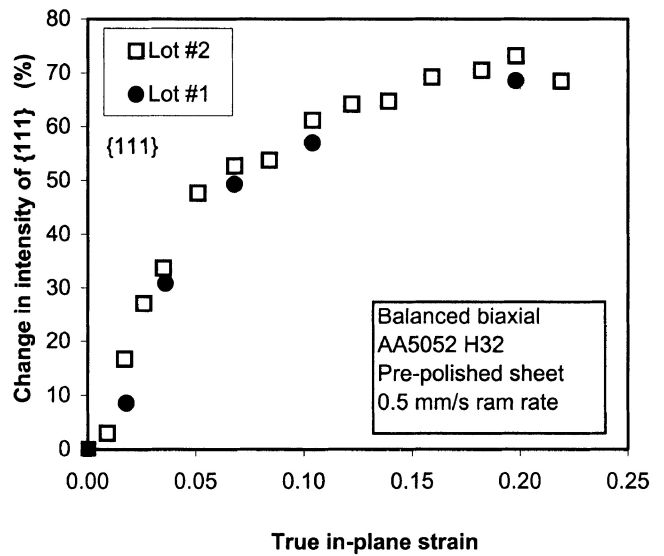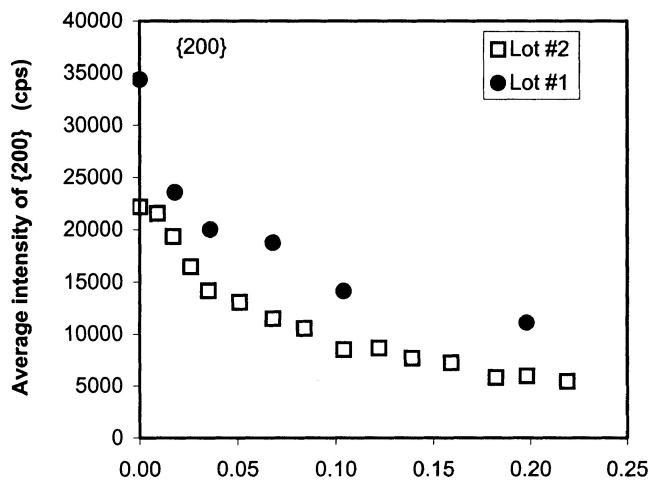
Fig. 9—Rocking curves obtained using X-ray diffraction for the three reflections (a) {111}, (b) {200}, and (c) {220}. Various strain levels are shown for samples from lot 1.
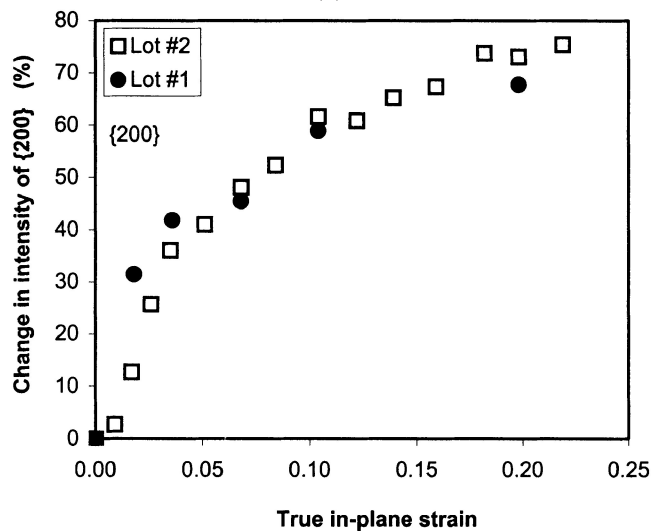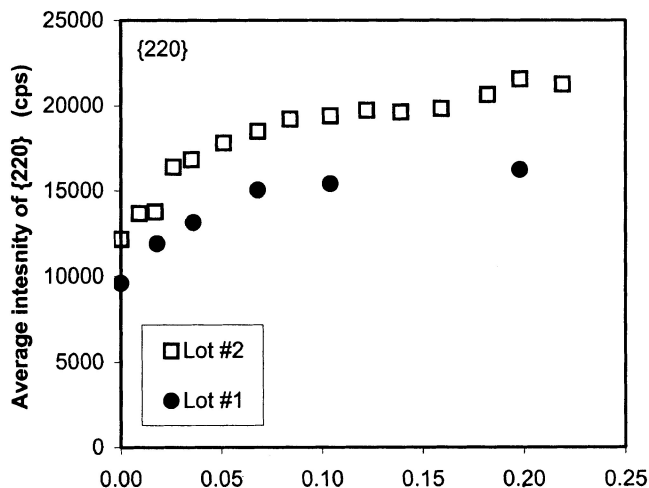
Fig. 10—Average intensities for $\omega = 0$ deg position as a function of strain for the individual reflections (a) {111}, (b) {200}, and (c) {220} from both lots of material.

Fig. 11—Quantitative changes in the orientation of the sheets when compared to the initial condition. The absolute values of the changes in maximum intensities at the symmetry point ($\omega = 0$ deg) are shown as a function of the strain level for both lots of material: (a) {111}, (b) {200}, and (c) {220}.

Table V. The Rate of Texture Development, in Percent Change in cps/ε_p, for the Two Lots of AA5052-H32 as Calculated from Figure 10 for Each Reflection; Correlation Coefficients for the Fit of the Data Are also Indicated

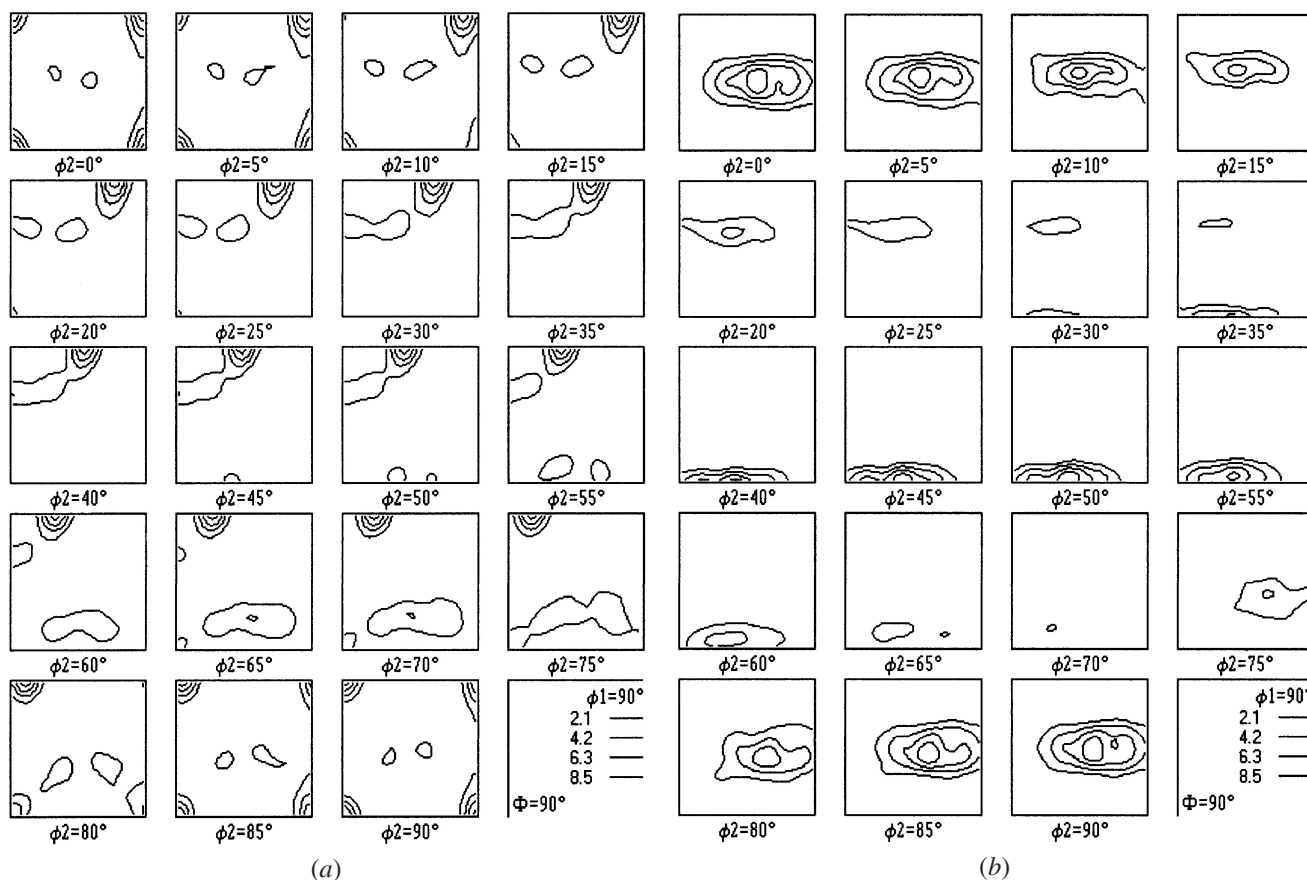| Analyzed Peak	Strain Levels ≤ 0.05		Strain Levels ≥ 0.05	
	Rate of Texture Development	Correlation Coefficient	Rate of Texture Development	Correlation Coefficient
111	992	0.98	161	0.96
200	923	0.90	189	0.95
220	934	0.96	151	0.96

Fig. 12—Orientation distribution function for material from lot 2: (*a*) as-received and (*b*) 0.219 strain level.

the crystals from plastic deformation will lead directly to the redistribution of crystallographic texture and changes in surface roughening. Many studies have been found which indicate the effect of strain on surface roughening[1–7] and texture[13,14,22–30] individually, but no one study has quantitatively tracked all three. In addition, the materials typically used in these experiments were fully recrystallized,[1,10,13,14,22,27] which annihilates the initial microstructure and texture of the sheet developed during rolling. From a technological point of view, it is essential to study these materials in the as-received condition, as this is the state in which they will be used in fabricating components.

A. *Development of Surface Roughness*

On a fundamental level, the cause of surface roughening is due to nucleation and movement of dislocations through the structure in order to accommodate straining of the material. However, the result of deformation typically manifested itself on a larger scale that has low-, medium-, and high-frequency components on a roughness profile. These various frequencies can be found in two different phases of roughening, identified by Wilson and Acselrad.[36] They are termed the microscopic and macroscopic phases of roughening. The microscopic phase encompasses the process of strain localization, in which inhomogeneities will localize on the scale of the microstructure. This occurs at the outset of straining, in which the grains most susceptible to deformation will develop slip bands within each individual grain (Figure 4). These bands contribute to the high-frequency portion of the roughness profile. While the number and severity of the slip bands increased with deformation, the in-grain surface roughness was observed to be on a much smaller scale than the grain-to-grain surface roughness. This latter portion of the roughness profile constitutes the medium-frequency range and typically comprises most of the roughness in the measured parameters.[4] Since strain is still somewhat localized at this stage, the grain-to-grain surface roughness

is also in the microstructural phase. As deformation of the material continues to increase, mismatch strains develop at the grain boundaries due to the different orientations of slip systems in adjacent grains.[2,4–7,10–13] In order to accommodate these strain incompatibilities, grains will begin to rotate with respect to each other. The resulting out-of-plane component of the relative rotation contributes to surface roughening at the free surface (Figure 5(a)), as the effects of mutual constraint are partially relaxed in this area. With continued deformation, the rotation is aggravated and the valleys become deeper and wider. Neighboring grains may also slide relative to each other, forming steps at the grain boundaries and increasing the surface topography as well.

Dai and Chang[4] studied roughness profiles from strained sheets and determined that the grain-to-grain roughness of a composite profile is the dominant factor that contributes to surface topography. They found that although the roughness computed for the high-frequency component (from slip bands) is roughly one-third of that computed for the composite profile, in fact, it contributes far less to the actual surface-roughness parameters than it appears (approximately 1 pct). This is primarily due to the fact that the roughness parameter for a composite profile is not a simple addition of the different frequency components. This indicates that the in-grain surface roughness caused by plastic deformation (*i.e.*, slip bands) is not the major factor in the measured surface-roughness parameters, but rather, the grain-to-grain interactions and their subsequent out-of-plane rotation are the primary components of the roughening. This reinforces the trend that the roughness parameters scale with the grain size of the material.[4–9]

As these microstructural-scale strain inhomogeneities (peaks and valleys) grow and coalesce with increased deformation, they eventually form coherent regions of strain concentration that span the sheet thickness. These features are similar to the roping or ridging inhomogeneities observed during other modes of deformation.[10,12] This now comprises the macroscopic phase of roughening. The wavelength of these defects (on the order of 1 mm) is much larger than the wavelength of the grain rotation and, concomitantly, has the lowest frequency of the surface roughening. The present experimental results indicate a steady, near-linear growth in surface roughness with plastic deformation and that a gradual change in the surface roughness occurred near the limiting strain (around 0.20). It was at these levels of strain that the diffuse grooves were visually observed on the surface parallel to the rolling direction prior to failure of the sheet. From the roughness plots (Figure 6), the parameters appeared to level off at these later stages of deformation. However, measurements from inside of the groove (parallel to the channel) show that the roughening continues to increase (diamond symbols in Figures 6(c) and (d)), similar to the findings of Kobayashi *et al.*[37] Increased roughness values due to the low-frequency component are not observed, due to the cutoff length used to define the roughness parameters. Thus, it appears that the sheet is no longer experiencing uniform deformation at this point, and that plane-strain conditions have been reached (within the groove). Continued deformation of the sheet leads to a gradual decrease in the strain of the material outside of the groove and an increase in the stretching of the material located within the groove. This process is manifested by the deepening of the grooves that

continue to roughen and the leveling off of the roughness parameters outside of this sheet defect.

B. *Evolution of Crystallographic Texture*

Plastic deformation of the sheet will lead to mismatch strains at the grain boundaries due to the different orientations of slip systems in adjacent grains.[2,4–7,10–13] In order to accommodate these strain incompatibilities, grains will rotate with respect to each other to orient themselves in more stable positions for deformation to occur.[14] Literature has shown that underbalanced biaxial stretching, the main component of the evolved texture from Al-based alloys, was represented as ⟨110⟩ parallel to the normal direction of the sheet.[26,28–30,38] By assuming this configuration, the grains are aligned for optimum slip conditions along their slip systems {111}⟨110⟩. Results from the diffraction experiments confirm that the initial cube texture component was found to deteriorate during biaxial stretching, and the weight of components in the alpha fiber increased relatively quickly. The strengthening of the {220} component parallel to the plane of the sheet was shown by the large initial slope in Figure 11. Once oriented near the fiber, the grain positions stabilize, and rotation as a result of deformation occurs at a slower rate (Table V). Similar textural evolutions were observed by Kohara[38] as well. Investigating a high-purity aluminum sheet, he found that a large distribution of grains were oriented within the alpha fiber after deformation and, additionally, contained a very strong component of brass {110}⟨112⟩.

It was previously reported that the relative grain rotation of a strained aluminum sheet increased linearly with plastic strain.[4] The results of Figure 11 clearly do not support this finding. Instead, orientations rotated very quickly toward the alpha fiber below a strain range of 0.04 to 0.05, after which the rate of texture development was observed to decrease. Dai and Chang hypothesized that at low strains (up to 0.04), plastic deformation is small and some grains tend to be bonded together to rotate as a group with respect to the other grains or grain groups. Thus, a larger number of grains would rotate together in unison. As the strain increases above this level, fewer and fewer grains remain bonded together, resulting in an apparently slower rate of rotation. Another possibility is that there are fewer grains not located in stable orientations at the later stages of deformation; thus, the apparent decrease in rotation rates at the higher strain levels. The rates of texture development also appear to be relatively fast (Table V) and high (nearly 75 pct at failure), considering that the maximum amount of deformation introduced in the plane of the sheet was 0.22. However, when considering that the largest strains take place in the thickness of the sheet and are upward of 0.40, the relatively high rate of texture development can be justified.

C. *Correlation of Surface Roughness and Crystallographic Texture*

Becker's analysis of various crystallographic textures showed the evolution of localized strain bands through the material thickness and their effect on surface topography development.[1] Three ideal texture components, strong cube,
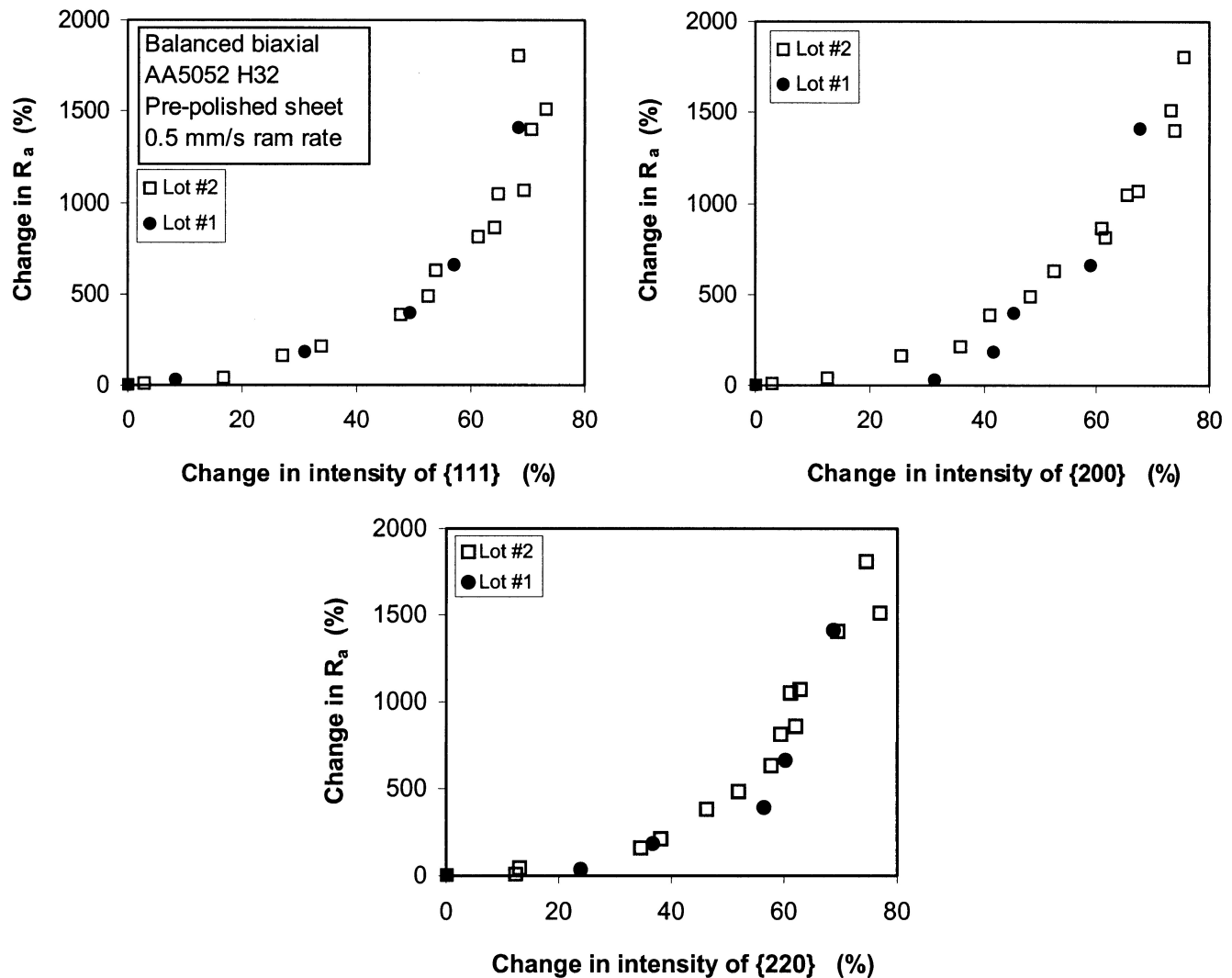
Fig. 13—Correlation between relative change in grain orientation and surface roughening for both lots of material.

strong Goss $\{011\}\langle001\rangle$, and an unstable $\{111\}[0\bar{1}1]$ orientation, were analyzed along with a recrystallized grain structure. From the numerical simulations, he observed that strain variations between localized regions and the immediate surroundings were much less for the strongly cube-textured sheet than for the other combinations. This resulted in a more uniform strain distribution along the surface and, subsequently, less roughening. Both the Goss and unstable configuration developed greater surface roughening, due in part to a significant amount of grain rotation early in deformation as a result of persistent bands of enhanced strain. From the results obtained in this study, the material that had the stronger $\{220\}$ component was found to roughen to a greater extent, even though the roughening rates of the two lots were equivalent (Figures 6(c) and (d)). This sheet was considered to have a stronger alpha fiber, which contains the Goss component. With this in mind, it is thought that Becker's results of greater surface roughening occurring with a strong Goss texturing may extend beyond just this single component to include other orientations within the alpha fiber. However, closer study of this fact is needed to indicate if these other orientations with their $\langle110\rangle$ component normal

to the rolling plane of the sheet are less favorable for evolved surface roughness as well.

From Figure 13, it can be seen that the higher degree of roughening from lot 2 was not based upon the relative change in grain orientation, as data from both lots tend to fall on the same curve. Since the difference in texturing of the material did not affect the rotation rate of the grains (Figure 11), the higher degree of roughening for lot 2 must be related to the localized interaction of the grains present in the material. For each strain increment, distortion of a grain is affected both by the crystallographic orientation of the grain and the local stress resulting from the deformation of neighboring grains.[7] Therefore, a grain of a given orientation could have a different imposed stress state with the same macroscopic deformation state if the surrounding texture was significantly different. Becker[1] showed this effect by rearranging the original recrystallized texture grains into three random combinations and analyzing the results. By changing the crystal orientations, the deformation incompatibility was enhanced and surface roughening increased over the original array. Therefore, reorganizing of grains with similar macroscopic textures can have a significant effect

upon the surface roughening. This grain-to-grain interaction may be the cause of the higher degree of roughening found for lot 2.

A final comment is made upon the difference between the macroscopic and microscopic phases of roughening, taking into consideration the anisotropy of the sheet. While the stress state was equibiaxial, the sheet was anisotropic in both a microstructural and crystallographic sense. This anisotropy of the sheet was observed only to affect the macroscopic phase of roughening, as aspects of the microscopic roughening were homogeneous (Figures 6(a) and (b)). This was seen in the preferred orientation of the diffuse grooves that developed parallel to the rolling direction. This phenomenon may be attributed to the mechanical fibering of the texture components along the rolling direction. This occurrence is not uncommon in aluminum alloys that have been thermomechanically processed. Previous work[13,39] has shown that segregation of textural components into elongated colonies consisting of grains with similar orientations was particularly damaging. This was due to the fact that colonies of grains with preferred orientations will deform differently than a group with random orientations and will eventually cause the strain to localize in a nonuniform manner. If the texture colony is softer than the matrix, it will tend to deform to a greater extent, providing a microstructural-scale plastic inhomogeneity that can grow and coalesce with others to form coherent regions of strain that span the thickness of the sheet. As solution-strengthened aluminum alloys are strain-rate-softening materials, this will result in necking and eventual failure. Marciniak and Kuczinski[15] based their approach describing tensile instabilities and eventual necking failure of "real" materials on strain inhomogeneities developed from local regions of weakness within the material such as this. Further, numerical simulations[12] have shown that grains having similar orientations can act collectively to form elevated or depressed regions during stretching. Therefore, it again brings to light the fact that statistical averaging conducted to obtain the crystallographic texture within the sheet provides useful trends for understanding the roughening rates of the material, but it does not appear to offer an adequate foundation for the prediction of the effects of crystallographic texture on surface roughness. Instead, the localized grain-to-grain or grain group–to–grain group interactions must be more closely studied.

V. CONCLUSIONS

From this investigation of balanced biaxial stretching in sheets of the aluminum alloy 5052-H32, the following conclusions were found.

1. The initial characteristics of the material from two different commercial lots of AA5052-H32 were found to be similar in terms of the microstructure (grain size, shape, and morphology of the second-phase constituent) and mechanical properties. However, X-ray diffraction techniques showed approximately a 30 pct difference between the crystallographic textures of the two heats.
2. The variation in texture of the two lots was observed to have an effect on the additional roughening of the surface subsequent to deformation. For a given lot of material, the surface roughness was proportional to the magnitude of the strain, and similar roughening rates were found

between the two sets of materials. However, the lot having a stronger initial {220} texture component was found to roughen to a higher degree.
3. The initial microstructural and crystallographic anisotropy of the sheet was found to have no effect on the microstructural roughening process. Macroscopically, diffuse grooves formed just prior to failure were found to orient themselves parallel to the rolling direction.
4. Relative changes in the sheet texture with plastic deformation were similar between the lots, with two rates of texture development occurring. For strains up to 0.05, the orientations were found to rotate quickly away from the cube {001}⟨100⟩ orientation observed in the as-received sheet toward positions along the α fiber (⟨011⟩ crystallographic direction parallel to the sheet normal). Subsequently, the {220} texture component continued to increase with deformation, but at a decreasing rate up to failure of the sheet.
5. The difference in the rate of texture development did not appear to have an effect on the surface roughening, as the relative change of the crystallographic orientations with increasing plastic strain was similar for both heats of material. It is believed that localized grain interactions may play a more important role in the surface roughening process.

REFERENCES

1. R. Becker: *Acta Mater.*, 1998, vol. 46 (4), pp. 1385-1401.
2. C. Guangnan, S. Huan, H. Shiguang, and B. Baudelet: *Mater. Sci. Eng.*, 1990, vol. 128A, pp. 33-38.
3. P.F. Thomson and P.U. Nayak: *Int. J. Mach. Tool Des. Res.*, 1980, vol. 20, pp. 78-86.
4. Y.Z. Dai and F.P. Chiang: *Trans. ASME*, 1992, vol. 114, pp. 432-38.
5. A. Azushima and M. Miyagawa: *J. Jpn. Soc. Technol. Plasticity*, 1986, vol. 27, pp. 1261-67.
6. D.V. Wilson, W.T. Roberts, and P.M.B. Rodrigues: *Metall. Trans. A*, 1981, vol. 12A, pp. 1595-1602.
7. K. Osakada and M. Oyane: *Bull. JSME*, 1971, vol. 14 (68), pp. 171-77.
8. M. Fukuda, K. Yamaguchi, N. Takakura, and Y. Sakano: *J. Jpn. Soc. Technol. Plasticity*, 1974, vol. 15, p. 994.
9. H. Kaga: *Ann. Coll. Int. Etud. Sci. Tech. Prod. Mec.*, 1971, vol. 20, pp. 55-67.
10. N.J. Wittridge and R.D. Knutsen: *Mat. Sci. Eng.*, 1999, vol. 269A, pp. 205-16.
11. W.R.D. Wilson and W. Lee: *Proc. 1st Int. Conf. on Tribology in Manufacturing Processes '97*, Gifu, Japan, 1997, pp. 71-76.
12. A.J. Beaudoin, J.D. Bryant, and D.A. Korzekwa: *Metall. Trans.*, 1998, vol. 29A, pp. 2323-32.
13. D.V. Wilson, W.T. Roberts, and P.M.B. Rodrigues: *Metall. Trans. A*, 1981, vol. 12A, pp. 1603-11.
14. R. Becker and S. Panchanadeeswaran: *Acta Mater.*, 1995, vol. 43 (7), pp. 2701-19.
15. Z. Maciniak and K. Kuczynski: *Int. J. Mech. Sci.*, 1967, vol. 9, pp. 609-20.

16. T.J. Foecke, S.W. Banovic, and R.J. Fields: *JOM*, 2001, vol. 53 (2), pp. 27-30.
17. C.S. Choi, H.J. Prask, and S.F. Trevino: *J. Appl. Crystallogr.*, 1979, vol. 12, pp. 327-331.
18. M.D. Vaudin: *Proc. 12th Int. Conf. on Textures of Materials*, J.A. Szpunar, in NRC Research Press, Ottawa, 1999, pp. 186-91.
19. M.D. Vaudin, M.W. Rupich, M. Jowett, G.N. Riley, and J.F. Bingert: *J. Mater. Res.*, 1998, vol. 13 (10), pp. 2910-19.
20. M.D. Vaudin: TexturePlus, http/:/www.ceramics.nist.gov/webbook/TexturePlus/texture.htm, 2000.
21. P.R. Dawson and A.J. Beaudoin: *JOM*, 1997, vol. 49 (9), pp. 34-41.
22. X.Y. Wen and W.B. Lee: *Scripta Mater.*, 2000, vol. 43 (1), pp. 1-7.
23. X.M. Cheng, Y. Liu, and J.G. Morris: *Alum. Trans.*, 1999, vol. 1 (1), pp. 103-08.
24. J.J. Park: *J. Mater. Proc. Technol.*, 1999, vol. 87 (1–3), pp. 146-53.
25. B. Ren, J.G. Morris, and A.J. Beaudoin: *JOM*, 1996, vol. 48 (6), pp. 22-25.
26. L.S. Toth, J. Hisch, and P. VanHoutte: *Int. J. Mech. Sci.*, 1996, vol. 38 (10), pp. 1117-26.
27. S. Panchanadeeswaran and D.P. Field: *Acta Mater.*, 1995, vol. 43 (4), pp. 1683-92.
28. Y. Zhou and K.W. Neale: *Acta Mater.*, 1994, vol. 42 (6), pp. 2175-89.
29. Y. Zhou and K.W. Neale: *Textures Microstr.*, 1993, vol. 22, pp. 87-111.
30. J.C. Starczan, D. Ruer, and R. Baro: *Proc. ICOTOM 6*, Iron and Steel Institute, Tokyo, 1981, pp. 308-316.
31. In *Aluminum: Properties and Physical Metallurgy*, J.E. Hatch, ed., ASM, Metals Park, OH, 1984, pp. 64-66.
32. S.S. Hecker: *J Eng. Mater.–Trans. ASME*, 1975, vol. 97 (1), pp. 66-73.
33. A.K. Ghosh and S.S. Hecker: *Metall. Trans.*, 1974, vol. 5, pp. 2161-64.
34. M. Huang and J.C. Gerdeen: in *Computer Applications in Shaping and Forming of Materials*, M.Y. Demeri, ed., TMS, Warrendale, PA, 1992, pp. 239-49.
35. J.C. Williams, A.W. Thompson, and R.G. Baggerly: *Scripta Metall.*, 1974, vol. 8, pp. 625-30.
36. D.V. Wilson and O. Acselrad: *Proc. IDDRG 10th Biennial Congr.*, Portcullis Press, Redhill, UK, 1978, vol. 155.
37. T. Kobayashi, K. Murata, and H. Ishigaki: *J. Jpn. Soc. Technol. Plasticity*, 1969, vol. 10, p. 793.
38. S. Kohara: *Proc. ICOTOM 6*, Iron and Steel Institute, Tokyo, 1981, pp. 300-07.
39. C.Y. Tang and W.H. Tai: *J. Mater. Proc. Technol.*, 2000, vol. 99, pp. 135-40.